
Feature Attribution with Necessity and Sufficiency via Dual-stage Perturbation Test for Causal Explanation

Xuexin Chen¹ Ruichu Cai^{*1} Zhengting Huang¹ Yuxuan Zhu¹ Julien Horwood² Zhifeng Hao³ Zijian Li⁴
José Miguel Hernández-Lobato²

Abstract

We investigate the problem of explainability in machine learning. To address this problem, Feature Attribution Methods (FAMs) measure the contribution of each feature through a perturbation test, where the difference in prediction is compared under different perturbations. However, such perturbation tests may not accurately distinguish the contributions of different features, when their change in prediction is the same after perturbation. In order to enhance the ability of FAMs to distinguish different features' contributions in this challenging setting, we propose to utilize the probability (PNS) that perturbing a feature is a necessary and sufficient cause for the prediction to change as a measure of feature importance. Our approach, Feature Attribution with Necessity and Sufficiency (FANS), computes the PNS via a perturbation test involving two stages (factual and interventional). In practice, to generate counterfactual samples, we use a resampling-based approach on the observed samples to approximate the required conditional distribution. Finally, we combine FANS and gradient-based optimization to extract the subset with the largest PNS. We demonstrate that FANS outperforms existing feature attribution methods on six benchmarks.

1. Introduction

Feature attribution is a method for explaining machine learning (ML) models by assigning weights to input features, where the absolute value of these weights denotes their con-

tribution to a model's prediction. Mathematically, suppose we have a function f that denotes a trained ML model, a target input $\mathbf{x}=(x_1, \dots, x_d)$ to be explained, and a baseline \mathbf{x}' , where x'_i is the approximate value that feature x_i would take if it were considered missing. An attribution of the prediction at input \mathbf{x} relative to \mathbf{x}' is a vector $\alpha_f(\mathbf{x}, \mathbf{x}')=(a_1, \dots, a_d)$, where a_i is the contribution of x_i to the prediction $f(\mathbf{x})$.

Standard feature attribution methods (FAMs) measure the contribution of each feature through a *perturbation* test, i.e., comparing the difference in prediction under different perturbations, or before and after the perturbation, where a subset of the variables of \mathbf{X} are set to their baseline values (Lundberg & Lee, 2017; Sundararajan et al., 2017). However, this perturbation test may not accurately distinguish the contribution of different features to the prediction when their change in prediction is the same after perturbation. To better understand this phenomenon, we provide an example as follows.

Example 1.1. Consider a binary classification model f for $\mathbf{X}=(X_1, X_2, X_3) \in \mathbb{R}^3$ that is captured by a function $Y=h(X_1, X_2, X_3)=\mathbb{I}(X_1-X_2>1)$, where Y is a binary variable representing true or false. Assuming that the baseline \mathbf{x}' is $(0, 0, 0)$, given the target input $\mathbf{x}=(1, 1, 1)$.

The attribution scores obtained from the existing FAMs for features x_1 and x_3 may both be 0 since the model's predictions given \mathbf{x} under different perturbations relative to \mathbf{x}' for any subset of \mathbf{X} are always equal to $h(\mathbf{x})$, which may misleadingly suggest that x_1, x_3 contribute equally to $h(\mathbf{x})$. Clearly, the contributions of x_1, x_3 are not equal, since the value of $h(\mathbf{x})$ is determined solely by the difference between x_1 and x_2 being less than 1, and is not influenced by x_3 . To solve this problem, we propose to use the Probability of Necessity and Sufficiency (PNS). Let s denote a subset of dimensions of \mathbf{X} . We measure the importance of the feature subsets of \mathbf{x} on s (denoted as \mathbf{x}_s , e.g., $\mathbf{x}_s=\{x_1, x_3\}$ for $s=\{1, 3\}$) by measuring the probability that perturbing \mathbf{x}_s is a necessary and sufficient cause for the prediction to change. Specifically, given any two events A_s and B_s , PNS measures the probability that event \bar{B} occurs when event \bar{A} occurs, and event B occurs when event A occurs (as the "if and only

^{*}Corresponding author ¹School of Computer Science, Guangdong University of Technology, Guangzhou 510006, China ²Department of Engineering, University of Cambridge, Cambridge CB2 1PZ, United Kingdom ³Shantou University, Shantou 515063, China ⁴Mohamed bin Zayed University of Artificial Intelligence, Masdar City, Abu Dhabi. Correspondence to: Ruichu Cai <cairuichu@gmail.com>.

Preliminary work.

if” of the relationship). In our context, we take event A as perturbing the features on s of different samples, which share the features \mathbf{x}_s and event B as prediction changes after perturbation. In Example 1.1, the PNS for x_3 (i.e. $s = \{3\}$) is 0, since perturbing x_3 is impossible to cause the prediction to change, while the PNS for x_1 may be greater than 0 because, for any sample that shares the value of x_1 , the prediction may change or remain unchanged when x_1 is perturbed or not perturbed.

Based on the above analysis, to enhance the ability of the FAMs to distinguish different feature contributions when the prediction changes are the same after perturbation, we present a Feature Attribution with Necessity and Sufficiency (FANS) method to measure the importance of each feature subset. First, to estimate PNS, we design a general perturbative prediction process of ML models accounting for input, prediction, and perturbation. Second, we calculate the PNS for each feature subset as its importance score. To achieve this goal, we first decompose PNS into a weighted sum of the probability that event A is a sufficient cause for event B (PS) and the probability that event A is a necessary cause for event B (PN). Then we design two dual-stage perturbation tests for PN and PS respectively. Specifically, to estimate PS, in the factual stage, we draw inputs from a distribution conditional on the fact that predictions remain unchanged after perturbing the features of \mathbf{X} on $\bar{\mathbf{S}}$, where $\mathbf{X}_{\bar{\mathbf{S}}}=\mathbf{x}_{\bar{\mathbf{S}}}$. In the interventional stage, we perturb the collected inputs on \mathbf{S} and count the proportion of prediction changes. Similarly, the perturbation test for PN is constructed by exchanging the perturbation and prediction events involved in the above two stages. Since the conditional distribution in the factual stage may be complex, we propose to use Sampling-Importance-Resampling on the observed inputs to approximate it. Further, we combine FANS and a gradient-based optimization method to extract the subset with the largest PNS. We demonstrate FANS outperforms existing FAMs on six benchmarks of image and graph data.

2. Related Work

2.1. ML Explainability

Explainable artificial intelligence (XAI) methods aim to provide human-readable explanations to help users comprehend and trust the outputs created by ML models. At present, a series of XAI methods have been developed, mainly including building interpretable models (e.g., linear regression model) and generating post hoc explanations. The post hoc explanation methods mainly include feature attribution methods (Yang et al., 2023b), which provide an estimate of the contribution of input features to a model’s prediction, example-based methods (Koh & Liang, 2017), which provide example(s) that may be considered similar or as prototype(s), hidden semantics (Simonyan et al., 2013), which

make sense of certain hidden neurons, etc. In this paper, we focus on the feature attribution approach.

Existing feature attribution methods (FAMs) mainly measure the contribution of features to prediction through a *perturbation* test, i.e., by perturbing the features and comparing the resulting differences in predictions. Typically, Shapley value-based methods (Shapley et al., 1953; Lundberg & Lee, 2017) measure the difference in a model’s predictions given data points with and without the feature included. Gradient-based methods (Sundararajan et al., 2017; Yang et al., 2023b) measure the rate of change in prediction corresponding to a tiny change in an input feature. LIME-based methods (Ribeiro et al., 2016; Dhurandhar et al., 2022) learn simplified, interpretable models on perturbed feature subsets. There are also many methods to find the feature subset with the highest contribution by optimizing a loss function between the L_p norm of an input feature mask and the prediction given the masked inputs (Tan et al., 2022; Fong & Vedaldi, 2017). However, current feature attribution methods may not accurately distinguish the contributions between different features when their change in prediction is the same after perturbation. To address this issue, FANS employs a dual-stage perturbation test, which has advantages in handling these cases.

2.2. Probability of Necessity and Sufficiency

PNS (Pearl, 2022) can be used to measure the “if and only if” of the relationship between two events and currently has many applications. For example, in ML explainability, LEWIS (Galhotra et al., 2021), LENS (Watson et al., 2021) and NSEG (Cai et al., 2022) use sufficiency or necessity to measure the contribution of input feature subsets. However, LEWIS uses only PS or PN, while LENS uses a variant of PS, so the attribution scores of these methods lack sufficient and necessary theoretical guarantees. NSEG extracts the feature subset with the largest PNS by introducing an identifiability assumption and then optimizing the lower bound of PNS, but our FANS does not require this assumption and directly uses PNS to measure the importance of each feature subset. In the out-of-distribution generalization problem, it can be used to extract domain-invariant information (Yang et al., 2023a). In the causal effect estimation problem, it can be used to learn individual responses from population data (Mueller et al., 2021).

3. Feature Attribution with Model Perturbative Prediction Process

Our goal is to quantify the impact of features on the resultant predictions by fixing certain features to values similar to those observed in a target input \mathbf{x} , and then allowing other features to change according to the data distribution. Figure 1 illustrates this process. Specifically, let \mathbf{X} denote the input

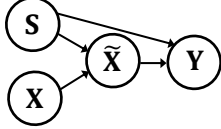


Figure 1. Model perturbative prediction process. \mathbf{S} denotes a subset of dimensions of \mathbf{X} for perturbation. $\tilde{\mathbf{X}}$ represents an input with fixed features on \mathbf{S} that are similar to the target input \mathbf{x} .

variable and \mathbf{S} denote a subset of dimensions on which to perturb the input, with $\bar{\mathbf{S}}$ denoting its complement. Sequentially, given a constant $b \geq 0$, define the distribution of \mathbf{X} with the condition that the L_p norm of the value of \mathbf{X} on \mathbf{S} with respect to the value of the target input \mathbf{x} is not greater than b . To avoid confusion, we represent the corresponding random variables that follow this conditional distribution as $\tilde{\mathbf{X}}$:

$$\tilde{\mathbf{X}} \sim P(\mathbf{X} \mid \|\mathbf{X}_{\mathbf{S}} - \mathbf{x}_{\mathbf{S}}\|_p \leq b). \quad (1)$$

Note that the conditional distribution in Eq. 1 can be obtained by sampling from the original input data distribution given a value of \mathbf{S} and retaining only the samples that satisfy the condition $\|\mathbf{X}_{\mathbf{S}} - \mathbf{x}_{\mathbf{S}}\|_p \leq b$. Finally, given the ML model f , a baseline \mathbf{x}' , a d -dimensional Bernoulli distribution with hyperparameter ϕ specified by the user (it is fixed to 0.5 in practice), let $\mathbf{1}$ denote an all-ones vector and we design a perturbation function g to randomly perturb the features of $\tilde{\mathbf{x}}$ specified by \mathbf{S} as follows.

$$g(\tilde{\mathbf{x}}, \mathbf{S}, \mathbf{x}') = (\mathbf{1} - \mathbf{m}_{\mathbf{S}}) \circ \tilde{\mathbf{x}}_{\mathbf{S}} + \mathbf{m}_{\mathbf{S}} \circ \mathbf{x}'_{\mathbf{S}}, \quad \mathbf{m} \sim \text{Bern}(\phi), \quad (2)$$

where \circ represents element-wise multiplication. The reason for the Bernoulli distribution introduced in Eq. 2 is that in the process of quantifying the model's predictions by the impact of perturbing the dimensions specified by \mathbf{s} , the dimensions that can influence the model predictions may be \mathbf{s} or a subset of \mathbf{s} . Therefore, we sample selected dimensions of \mathbf{s} to obtain a more comprehensive quantification. Further, we use $\mathbf{Y} = f(g(\tilde{\mathbf{x}}, \mathbf{S}, \mathbf{x}'))$ to denote the process of perturbing the values of $\tilde{\mathbf{x}}$ and then predicting.

Remark 3.1. Our model perturbative prediction process differs from the standard causal generation process in two ways. First, variable \mathbf{Y} is the model's prediction rather than a property of the real-world data. Second, by intervening on a variable in our process, the outcome of its corresponding children's variables is available.

Given any model f , the goal of feature attribution can be formalized with the help of the aforementioned perturbative prediction process. Specifically, given a d -dimensional vector \mathbf{x} , we let $z(\mathbf{x}, \mathbf{s})$ be a perturbative prediction process, so the goal of feature attribution is to devise a score function $\phi : z, x_{\mathbf{s}} \rightarrow w_{\mathbf{s}}$, such that this score function ϕ is able to distinguish features with significantly different contributions to model predictions.

4. Feature Attribution as a Problem of PNS Measurement

Based on the previous problem definition, we find that the goal of feature attribution is to find a score function g that can distinguish features with significantly different contributions to model predictions. However, it is not a trivial task since the degree of change in predictions and the contribution of features to predictions may be asymmetric.

To solve this problem, one straightforward intuition is to describe the features that influence the prediction if and only if they are present, which can be addressed with the help of the probability of necessity and sufficiency. Therefore, we reformalize PNS as follows. Suppose f is a binary classification model. Standard feature attribution methods measure the contribution of each feature to the prediction by comparing different perturbations of the feature \mathbf{x} , which involves two events $A_{\mathbf{s}}, B_{\mathbf{s}}$. Specifically, we let $A_{\mathbf{s}}$ denote an event of *perturbation on the feature subset \mathbf{s} of \mathbf{X} relative to \mathbf{x}'* and $B_{\mathbf{s}}$ denote an event of *prediction change on the prediction y with $|y' - y| > c$ and y' is the value of y after some perturbation on the subspace \mathbf{s} relative to \mathbf{x}'* . Overloading the notation, we let $A_{\mathbf{s}}$ be the feature with the index of \mathbf{s} that is perturbed, and $B_{\mathbf{s}}$ be the label that is changed after some perturbations. Moreover, we have the following definitions (Pearl, 2022).

Definition 4.1. (Probability of necessity, PN)

$$PN = P(\bar{B}_{\mathbf{s}} | A_{\mathbf{s}}, B_{\mathbf{s}}), \quad (3)$$

PN is the probability that, given that events $A_{\mathbf{s}}$ and $B_{\mathbf{s}}$ both occur initially, event $B_{\mathbf{s}}$ does not occur after event $A_{\mathbf{s}}$ is changed from occurring to not occurring.

Definition 4.2. (Probability of sufficiency, PS)

$$PS = P(B_{\mathbf{s}} | \bar{A}_{\mathbf{s}}, \bar{B}_{\mathbf{s}}) \quad (4)$$

PS is the probability that, given that events $A_{\mathbf{s}}$ and $B_{\mathbf{s}}$ both did not occur initially, event $B_{\mathbf{s}}$ occur after event A is changed from not occurring to occurring.

Definition 4.3. (Probability of necessity and sufficiency, PNS)

$$PNS = PN \cdot P(A_{\mathbf{s}}, B_{\mathbf{s}}) + PS \cdot P(\bar{A}_{\mathbf{s}}, \bar{B}_{\mathbf{s}}) \quad (5)$$

PNS is the sum of PN and PS, each multiplied by the probability of its corresponding condition. PNS measures the probability that event $A_{\mathbf{s}}$ is a necessary and sufficient cause for event $B_{\mathbf{s}}$.

When evaluating the feature weight $w_{\mathbf{s}}$ in a certain input, if we hope that $w_{\mathbf{s}}$ can reflect the probability that perturbing $x_{\mathbf{s}}$ is a sufficient and necessary cause of prediction change, then this $w_{\mathbf{s}}$ can be defined as:

$$w_{\mathbf{s}} = P(\bar{B}_{\mathbf{s}} | A_{\mathbf{s}}, B_{\mathbf{s}}) \cdot P(A_{\mathbf{s}}, B_{\mathbf{s}}) + P(B_{\mathbf{s}} | \bar{A}_{\mathbf{s}}, \bar{B}_{\mathbf{s}}) \cdot P(\bar{A}_{\mathbf{s}}, \bar{B}_{\mathbf{s}}). \quad (6)$$

Therefore, in order to calculate the target score as shown in Eq. 6, it can be broken down into the calculation of four probabilities, where $P(A_s, B_s)$ and $P(\bar{A}_s, \bar{B}_s)$ are the observation probabilities, and $P(\bar{B}_{\bar{A}_s} | A_s, B_s)$ and $P(B_{s_{A_s}} | \bar{A}_s, \bar{B}_s)$ are the counterfactual probabilities PN and PS, respectively. To facilitate calculation, we further formalize PN and PS into the following forms.

$$P(\bar{B}_{\bar{A}_s} | A_s, B_s) = \mathbb{E}_{\mathbf{x} \sim P(\tilde{\mathbf{X}} | A_s, B_s)} [P(|f(g(\mathbf{x}, \bar{\mathbf{s}}), \mathbf{x}') - f(\mathbf{x})| \leq c)_{\text{do}(\tilde{\mathbf{X}}=\mathbf{x})}], \quad (7)$$

$$P(B_{s_{A_s}} | \bar{A}_s, \bar{B}_s) = \mathbb{E}_{\mathbf{x} \sim P(\tilde{\mathbf{X}} | \bar{A}_s, \bar{B}_s)} [P(|f(g(\mathbf{x}, \mathbf{s}), \mathbf{x}') - f(\mathbf{x})| > c)_{\text{do}(\tilde{\mathbf{X}}=\mathbf{x})}], \quad (8)$$

where $\text{do}(\tilde{\mathbf{X}}=\mathbf{x})$ represents an intervention on variable $\tilde{\mathbf{X}}$ that fixes the value as \mathbf{x} . Note that event A not occurring is approximated by the complementary feature set \bar{s} . $P(\bar{B}_{\bar{A}_s} | A_s, B_s)$ and $P(B_{s_{A_s}} | \bar{A}_s, \bar{B}_s)$ will be calculated by the necessity and sufficiency modules in Section 5.

5. Necessary and Sufficient Attribution Estimation via Dual-stage Perturbation Test

5.1. Overview

Based on the definitions of necessary and sufficient attribution, we propose a Feature Attribution with Necessity and Sufficiency (FANS) method to extract the feature subset with the highest PNS, as shown in Figure 2. FANS consists of necessity modules and sufficiency modules, each performing our proposed dual-stage (factual and interventional stage) perturbation test to estimate PN and PS respectively. Since the conditional distributions involved in the factual stage may be complex, FANS adopts the sampling-importance-resampling (SIR) method to approximate these distributions with observed samples. Finally, FANS integrates the outputs of both modules into PNS and optimizes the perturbation. FANS assumes that the function f is a classification model with the probability of each class as output.

5.2. Dual-stage Perturbation Test

We design two different dual-stage perturbation tests to estimate the PS in Eq. 8 and PN in Eq. 7, respectively, by following the Abduction-Action-Prediction counterfactual reasoning paradigm (Pearl, 2013). Abduction involves setting conditions for specific variables (corresponds to $\tilde{\mathbf{X}}$ in our context) based on the observations (corresponds to prediction \mathbf{Y} given a perturbation \mathbf{S}). The action involves intervening in the values of certain variables (corresponds to $\mathbf{S}, \tilde{\mathbf{X}}$). Prediction involves computing the resulting conditional predictive distribution. This corresponds to the conditional distribution for \mathbf{Y} given intervention value of \mathbf{S} and the values of $\tilde{\mathbf{X}}$ that satisfy the factual observations.

We first present the dual-stage perturbation test for PS. **1) (Factual stage)** Draw inputs from a distribution conditional on the fact that predictions remain unchanged after using the perturbation function (Eq. 2) to perturb the features of $\tilde{\mathbf{X}}$ on \bar{s} . **2) (Interventional stage)** Remove all arrows pointing to $\tilde{\mathbf{X}}$ in Figure 1 (i.e., perform the “do” operator in causality). For each collected sample on the feature s , use the perturbation function in Eq. 2 to randomly perturb multiple times and calculate the proportion of prediction changes. Finally, average the proportion of prediction changes for each input.

Similarly, the dual-stage perturbation test for PN is constructed by exchanging the perturbations and prediction events involved in the above two stages respectively.

5.3. Sufficiency Module

In this part, we provide a description of how to estimate probability of sufficiency with the help of our sufficiency module.

5.3.1. FACTUAL STAGE

To generate samples from $P(\tilde{\mathbf{X}} | \bar{A}_s, \bar{B}_s)$ in Eq. 8, we propose to apply SIR on the observed sample set \mathcal{E} that follows $P(\mathbf{X})$ to approximate the required conditional distribution. First, given perturbation \bar{s} , the resampling weight for each observed sample is as follows (detailed derivation can be found in Appendix A). Letting r denote a normalization constant, the SIR-based resampling weight of $\mathbf{v} \sim P(\mathbf{X})$ is given by

$$w_{\text{SF}}(\mathbf{x}) = \begin{cases} r \cdot P(|f(g(\mathbf{x}, \bar{\mathbf{s}}), \mathbf{x}') - f(\mathbf{x})| \leq c | \mathbf{x}), & \text{if } \|\mathbf{x}_s - \mathbf{x}'_s\|_p \leq b \\ 0, & \text{otherwise.} \end{cases} \quad (9)$$

Hence, the resampling weight of \mathbf{x} is determined by two conditions: $\|\mathbf{x}_s - \mathbf{x}'_s\|_p \leq b$ and $|f(g(\mathbf{x}, \bar{\mathbf{s}}), \mathbf{x}') - f(\mathbf{x})| \leq c$. To enhance the smoothness of the weight output from $w_{\text{SF}}(\cdot)$, we introduce the Gaussian kernel function to soften the above two conditions and take the product of their outputs as an approximation of the resampling weight $w_{\text{SF}}(\mathbf{x})$ of $\mathbf{x} \sim P(\mathbf{X})$, as follows.

$$\tilde{w}_{\text{SF}}(\mathbf{x}) := \exp\left(\frac{\|\mathbf{x}_s - \mathbf{x}'_s\|_p^2}{-2b^2}\right) \cdot \exp\left(\frac{|f(g(\mathbf{x}, \bar{\mathbf{s}}), \mathbf{x}') - f(\mathbf{x})|^2}{-2c^2}\right), \quad (10)$$

where the thresholds b, c are used as the bandwidths of the Gaussian kernel. Further, we feed observed samples and their weight according to Eq. 12 into the SIR algorithm, and the sample set that approximates the conditional distribution $P(\tilde{\mathbf{X}} | \bar{A}_s, \bar{B}_s)$ in PS (Eq. 8) can be obtained.

5.3.2. INTERVENTION STAGE

Let \mathcal{E}_{SF} be a sample set obtained through SIR in the factual stage of our Sufficiency Module. Then, PS (Eq. 8) can be

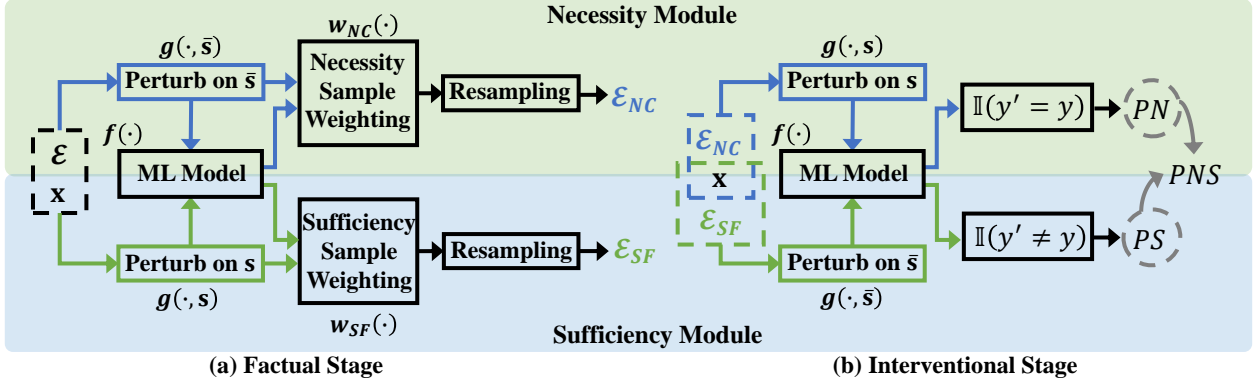


Figure 2. Architecture of FANS, which takes the sample \mathbf{x} to be explained and the samples $\mathcal{E} \stackrel{\text{iid}}{\sim} P(\mathbf{X})$ as inputs, throughout the necessity and sufficiency modules to output PN and PS, respectively, and finally combine PN, PS into PNS for optimization of perturbation \mathbf{s} . Each module consists of the following two stages. 1) Factual stage. Generate samples \mathcal{E}_{NC} and \mathcal{E}_{SF} conditional on the fact that the model’s predictions change or remain unchanged respectively after performing different perturbations. 2) Intervention stage. Apply perturbations different from the facts to \mathcal{E}_{NC} and \mathcal{E}_{SF} , and count the proportion of changes in the model’s prediction.

estimated as follows:

$$\hat{\text{PS}} = \frac{1}{|\mathcal{E}_{\text{SF}}| \cdot t} \sum_{\mathbf{x} \in \mathcal{E}_{\text{SF}}} \sum_{j=1}^t \mathbb{I}(|f(g(\mathbf{x}, \mathbf{s}, \mathbf{x}')) - f(\mathbf{x})| > c), \quad (11)$$

where the constant t denotes the number of perturbations.

5.4. Necessity Module

The implementation of the sufficiency module is similar to the necessity module, with the only difference being the opposite given perturbation and prediction events in each stage. Thus, in the factual stage, the SIR-based resampling weight for the observed sample $\mathbf{x} \sim P(\mathbf{X})$, which is used to generate the sample set that approximates the conditional distribution $P(\bar{\mathbf{X}} | A_{\mathbf{s}}, B_{\mathbf{s}})$ in Eq. 7, is given by

$$\tilde{w}_{\text{NC}}(\mathbf{x}) := \exp\left(\frac{\|\mathbf{x}_{\mathbf{s}} - \mathbf{x}'_{\mathbf{s}}\|_p^2}{-2b^2}\right) \cdot \left(1 - \exp\left(\frac{|f(g(\mathbf{x}, \mathbf{s}, \mathbf{x}')) - f(\mathbf{x})|^2}{-2c^2}\right)\right). \quad (12)$$

Further, let \mathcal{E}_{NC} be a sample set obtained through SIR in the factual stage of Necessity Module. Then PN (Eq. 7) can be estimated as follows:

$$\hat{\text{PN}} = \frac{1}{|\mathcal{E}_{\text{NC}}| \cdot u} \sum_{\mathbf{x} \in \mathcal{E}_{\text{NC}}} \sum_{j=1}^u \mathbb{I}(|f(g(\mathbf{x}, \mathbf{s}, \mathbf{x}')) - f(\mathbf{x})| \leq c), \quad (13)$$

where the constant u denotes the number of perturbations.

5.5. Optimization

In this section, we aim to maximize the estimated PNS with respect to perturbation \mathbf{s} by utilizing gradient-based optimization algorithms.

As mentioned in Section 4, since probability $P(A_{\mathbf{s}}, B_{\mathbf{s}})$ (or $P(\bar{A}_{\mathbf{s}}, \bar{B}_{\mathbf{s}})$) can be expressed as the weighted sum of conditional probabilities $P(A_{\mathbf{s}}, B_{\mathbf{s}} | \mathbf{x})$ with respect to all possible

\mathbf{x} , where the weight is $P(\mathbf{X})$, we can estimate $P(A_{\mathbf{s}}, B_{\mathbf{s}})$ and $P(\bar{A}_{\mathbf{s}}, \bar{B}_{\mathbf{s}})$ by summing their SIR-based weights of the observed samples in Eq. 12 and Eq. 10 respectively, as follows. Given the sample set \mathcal{E} that are independently drawn from the distribution $P(\mathbf{X})$,

$$\hat{P}(A_{\mathbf{s}}, B_{\mathbf{s}}) = \sum_{\mathbf{x} \in \mathcal{E}} w_{\text{NC}}(\mathbf{x}), \quad \hat{P}(\bar{A}_{\mathbf{s}}, \bar{B}_{\mathbf{s}}) = \sum_{\mathbf{x} \in \mathcal{E}} w_{\text{SF}}(\mathbf{x}) \quad (14)$$

Second, to optimize Eq. 5 with respect to perturbation \mathbf{s} , we can use a gradient-based algorithm (e.g., stochastic gradient descent) for optimization. Given the discrete nature of the set \mathbf{s} , we can first encode it as a binary vector containing d dimensions, and then relax the entries in the discrete set $\{0, 1\}$ into the continuous range $[0, 1]$. Additionally, we use $\mathbf{1} - \mathbf{s}$ to represent the complement of \mathbf{s} , where $\mathbf{1}$ is an all-ones vector. Further, we replace $\|\mathbf{x}_{\mathbf{s}} - \mathbf{x}'_{\mathbf{s}}\|_p$ in Eq. 9 with $\|\mathbf{x} \circ (\mathbf{1} - \mathbf{s}) - \mathbf{x}' \circ (\mathbf{1} - \mathbf{s})\|_p$, where \mathbf{s} is now a relaxed binary vector and \circ is a element-wise multiplication. Similarly, we replace $(\mathbf{1} - \mathbf{m}_{\mathbf{s}}) \circ \bar{\mathbf{X}}_{\mathbf{s}} + \mathbf{m}_{\mathbf{s}} \circ \mathbf{x}'_{\mathbf{s}}$ in Eq. 2 with $(\mathbf{1} - \mathbf{m}) \circ \bar{\mathbf{X}} \circ \mathbf{s} + \mathbf{m} \circ \mathbf{x}' \circ \mathbf{s}$. In addition, the indicator function $\mathbb{I}(|f(\cdot) - f(\cdot)| > c)$ in Eq. 11 is not differentiable, thus we replace it with the smooth function $1 - \exp(-|f(\cdot) - f(\cdot)|)$ to indicate whether the prediction changes. Similarly, $\mathbb{I}(|f(\cdot) - f(\cdot)| \leq c)$ in Eq. 13 is replaced with $\exp(-|f(\cdot) - f(\cdot)|)$.

Finally, after the optimization with respect to \mathbf{s} is completed by maximizing Eq. 5, the resultant values of \mathbf{s} will be utilized as weights assigned to various features.

6. Experiments

6.1. Experimental Setup

1) **Datasets and models.** We utilized six public datasets with well-trained models: CIFAR10 (Krizhevsky et al., 2009) with ResNet18, MNIST (LeCun et al., 1998) and Fashion-MNIST (Xiao et al., 2017) with LeNet5, as well

Feature Attribution with Necessity and Sufficiency via Dual-stage Perturbation Test for Causal Explanation

Table 1. Performance on the image datasets. The best performance is marked in bold, and the second best is underlined. Symbols \uparrow and \downarrow respectively represent that larger and smaller metric values are better.

Method	MNIST				Fashion-MNIST				CIFAR10			
	INF \downarrow	IR \uparrow	SPA \uparrow	MS \downarrow	INF \downarrow	IR \uparrow	SPA \uparrow	MS \downarrow	INF \downarrow	IR \uparrow	SPA \uparrow	MS \downarrow
Saliency	3.8×10^4	64.3	0.658	0.623	1.8×10^6	25.5	0.558	0.753	1.2×10^8	54.1	0.492	0.736
IG	<u>1.7×10^3</u>	<u>73.3</u>	<u>0.918</u>	0.683	<u>1.7×10^4</u>	<u>60.8</u>	0.612	0.806	1.5×10^5	<u>63.5</u>	0.631	0.966
DeepLift	<u>2.2×10^3</u>	<u>73.3</u>	<u>0.918</u>	0.679	<u>8.2×10^4</u>	<u>59.8</u>	0.610	0.797	1.9×10^5	62.7	0.631	0.959
IDGI	2.0×10^3	64.7	0.837	0.578	2.6×10^4	58.2	0.593	0.781	<u>2.3×10^4</u>	19.5	<u>0.632</u>	0.854
GradShap	2.2×10^3	<u>73.3</u>	<u>0.918</u>	0.673	2.5×10^4	59.2	<u>0.614</u>	0.874	2.3×10^5	56.5	0.630	1.000
LIME	6.6×10^5	67.9	0.808	0.899	2.5×10^8	28.6	0.533	0.884	1.1×10^9	2.1	0.512	1.032
Occlusion	5.7×10^5	69.2	0.802	<u>0.538</u>	2.8×10^7	58.4	0.505	0.660	2.1×10^8	51.4	0.507	0.857
FeatAblation	<u>1.7×10^3</u>	72.8	0.917	0.669	5.5×10^4	45.4	0.572	0.791	1.1×10^6	36.8	0.619	0.983
MP	<u>8.5×10^5</u>	70.3	0.421	0.904	2.9×10^7	20.1	0.227	0.453	5.1×10^8	16.3	0.476	0.887
CIMI	1.7×10^4	12.9	0.901	0.548	2.6×10^4	54.8	0.589	0.827	6.0×10^6	21.1	0.589	<u>0.615</u>
FANS	9.0×10^2	74.5	0.924	0.463	1.2×10^4	63.1	0.630	<u>0.586</u>	1.7×10^4	63.6	0.634	0.578

as BACommunity, Pubmed, and Citeseer with GCN (Ying et al., 2019; Sen et al., 2008; Kipf & Welling, 2016). CIFAR10, MNIST, and Fashion-MNIST are image datasets. BACommunity, Pubmed, and Citeseer are graph datasets. Please see Appendix B.1 for details.

2) **Baselines.** We compared FANS with six feature-wise attribution methods: Saliency (Simonyan et al., 2014), GuidedBP (Springenberg et al., 2015), IntegratedGrad(IG) (Sundararajan et al., 2017), GradShap (Lundberg & Lee, 2017), DeepLift (Ancona et al., 2018), and IDGI (Yang et al., 2023b), as well as nine feature subset-wise attribution approaches: Occlusion (Zeiler & Fergus, 2014), LIME (Ribeiro et al., 2016), MeaningfulPerturb(MP) (Fong & Vedaldi, 2017), GNNExplainer (Ying et al., 2019), PGExplainer (Luo et al., 2020), FeatAblation (Kokhlikyan et al., 2020), ReFine (Wang et al., 2021), CFGNExplainer (Lucic et al., 2022), CF² (Tan et al., 2022), CIMI (Wu et al., 2023) and MixUpExplainer (Zhang et al., 2023). The data categories used to test each baseline are largely aligned with their literature. Except that we adjust CIMI to accommodate image data, and run Saliency, GuidedBP, and IG on both graph and image data. Please see Appendix B.2 for details.

3) **Evaluation Metrics.** We utilized six widely used metrics to evaluate the effectiveness of FANS: Infidelity(INF) (Yeh et al., 2019), Iterative Removal Of Features(IR) (Rieger & Hansen, 2020), Fidelity⁺(FID⁺), Fidelity⁻(FID⁻) (Amara et al., 2022), Max-Sensitivity(MS) (Yeh et al., 2019), Sparseness(SPA) (Chalasanani et al., 2020), and Recall@12 (Wang et al., 2021) metrics. INF, IR, FID⁺, and FID⁻ measure the extent to which the explanation follows the predicted behavior of the model (i.e., faithfulness), while MS measures the stability of the explanation when subjected to slight input perturbations (i.e., robustness) (Hedström et al., 2023). SPA measures the sparsity of the explanation by using the Gini Index. Recall@12 measures how many of the top 12 most important features for a given attribution are features of the “ground-truth explanation”. Remarkably, Recall@12 is only suitable for BACommunity since this dataset is syn-

thetic and contains “ground-truth explanation”. Please see Appendix B.3 for details.

To test the explanation methods, we randomly selected 4,000 images from each image dataset (i.e., MNIST, Fashion-MNIST, and CIFAR10) and adopted the same configuration as the literature (Wang et al., 2021) on the graph datasets (i.e., BACommunity, Citeseer, and Pubmed). The results presented in Tables 1 and 2 are largely averages of the metric values for the different inputs, with the exception of FID⁺ and FID⁻, since these are metrics designed for the entire dataset rather than an individual sample. As each graph dataset we use contains only one graph, and FANS requires multiple samples for SIR, we create a graph-augmented dataset for each graph by randomly masking their adjacency matrix. More implementation details are presented in Appendix B.4.

6.2. Explanation Evaluation

6.2.1. QUANTITATIVE EVALUATION

Performance comparison. We verify the experimental performance of FANS against the state-of-the-art baselines in Tables 1 and 2. As shown in Table 1, FANS significantly and consistently outperforms all the baselines in terms of faithfulness, sparsity, and robustness on different image datasets. In particular, we find that: 1) For the faithfulness metric INF, FANS outperforms the second-best approach by 47.06%, 29.41%, and 26.09% on MNIST, Fashion-MNIST, and CIFAR10. For IR, FANS improves by 1.64%, 3.78%, and 0.16%. These results indicate that extracting necessary and sufficient causes for input predictions can effectively capture key subsets of features that influence the model’s predictive behavior. 2) For the sparsity metric SPA, FANS outperforms the next best method by 0.65%, 2.61%, and 0.32% on the three image datasets. This validates that FANS’s necessity module, which adaptively removes unimportant features by randomly masking them, outperforms other methods in terms of attribution sparsity. 3) For the robustness metric MS, FANS outperforms the second-best method by 13.94%

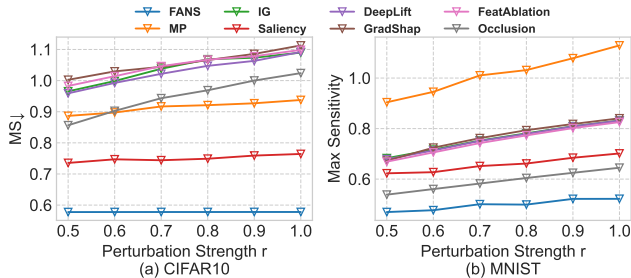


Figure 3. Performance on robustness comparison in image datasets CIFAR10 and MNIST under different perturbation strengths.

and 6.02% on the MNIST and CIFAR10 datasets, while achieving a somewhat lower but still competitive MS result on Fashion-MNIST. We find that FANS significantly outperforms gradient-based methods, probably due to the sensitivity of gradients to noisy feature values. FANS learns from a set of similar features obtained through SIR, which helps it to mitigate the effects of noise.

Similarly, in Table 2, FANS regularly surpasses all the baselines on the graph datasets. In particular, in terms of FID+, FANS improves by 4.99% on BACommunity, 46.15% on Citeseer, and 13.33% on Pubmed relative to the baselines. It provides further modest improvements with respect to the sparsity metric SPA. For another faithfulness metric FID-, FANS is the only method achieving optimal values (i.e., 0) across all three datasets. FANS outperforms other approaches for Citeseer and Pubmed while remaining competitive on Recall@12 for the synthetic BACommunity dataset.

Robustness analysis. Next, we investigate the robustness of FANS and the baseline methods by examining the effect of introducing noise. Following the literature (Yeh et al., 2019), we designed a robustness experiment as follows. Given various values of r , for $r \in [0, 1]$, we add noise to each pixel of input image x_i from the interval $[-r, r]$. We then evaluate the difference between the explanations of each perturbed image and its original explanation via the Max Sensitivity (MS) metric. As shown in Fig.3(a)(b), as expected, all methods demonstrate a gradual deterioration in performance with increased perturbation strength. However, the slope of this deterioration is considerably lower using FANS, which demonstrates far superior robustness on both examined datasets. This can be explained by the fact that FANS learns from multiple samples which are similar to the target input through SIR, rather than a single sample, which renders it more robust to perturbation noise.

6.2.2. QUALITATIVE EVALUATION

In Figure 5, we visualize the attributions obtained for FANS and other baselines on five samples from the MNIST dataset. We find that the attributions of FANS and IG are more sparse than other methods. Compared to IG, FANS improves the contrast between the scores of important and unimportant features. This is visually demonstrated by a higher number

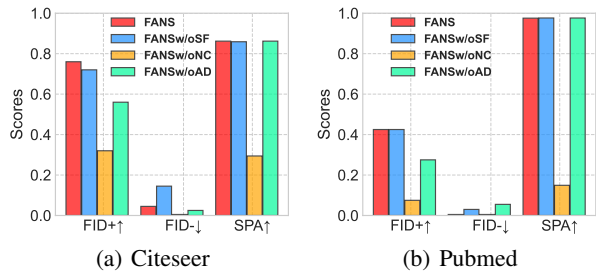


Figure 4. Ablation study of sufficiency (SF) module, necessity (NC) module, and SIR-based Abduction (AD) on graph datasets Citeseer and Pubmed.

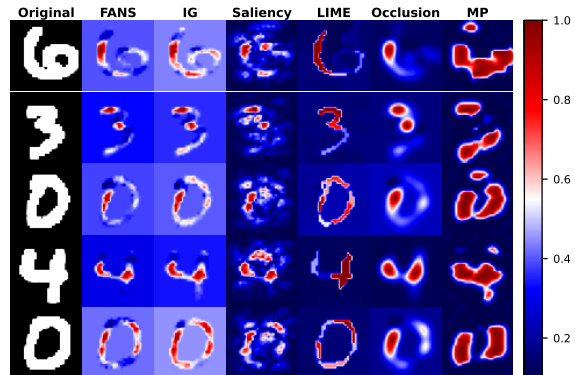


Figure 5. Attributions visualization on the MNIST dataset.

of blue pixels in FANS than in IG, which is expected since FANS’s PNS is used to attribute the sparsest and the most influential feature subset for the model’s predictions.

6.3. Ablation study

The core components of FANS are the necessity, sufficiency, and SIR-based Resampling modules. In order to validate the importance of each component and better understand their relationship to different explainability metrics, we ablate our method by iteratively removing each component. We refer to FANS without the sufficiency module as FANSw/oSF, FANS without the necessity module as FANSw/oNC, and FANS without SIR-based Resampling as FANSw/oSR. We visualize the effects of this ablation on performance relative to the full algorithm in Figure 4 for the Citeseer and Pubmed datasets. In Figure 4(a)(b), we first remark that the full FANS algorithm is the only version of the method to perform uniformly well across both datasets and all metrics. When comparing with FANSw/oSF, we notice a slight decrease in the faithfulness metric FID+ and a significant decrease in FID-, while the sparsity metric remains stable, where FID- and FID+ evaluate the proportions of predictions remain unchanged and change when features with high attribution scores are retained and removed, respectively. Conversely, FANSw/oNC exhibits an opposite trend to the above three metrics of FANSw/oSF, with FID+ becoming significantly worse, FID- remaining stable, and SPA becoming worse. This result is expected since the sufficiency and

Table 2. Performance on the graph datasets.

Method	BACommunity				Citeseer			Pubmed		
	FID ⁺ ↑	FID ⁻ ↓	SPA↑	Recall@12↑	FID ⁺ ↑	FID ⁻ ↓	SPA↑	FID ⁺ ↑	FID ⁻ ↓	SPA↑
Saliency	0.6667	0.1000	0.8899	0.5141	0.1800	0.0400	0.7476	0.0250	0.0250	0.9670
GuidedBP	0.4833	0.1000	0.9137	0.3822	0.0607	0.1207	0.8410	0.0000	0.0250	0.9629
IG	0.6667	0.1167	0.9200	0.5204	0.5200	0.0400	0.8380	0.0250	0.0000	0.9636
GNNExplainer	0.4000	0.0667	0.6432	0.4210	0.1821	0.0000	0.3760	0.0750	0.0000	0.6058
PGExplainer	0.4667	0.0500	0.8092	0.6025	0.4292	0.2800	0.1435	0.0258	0.0250	0.01380
ReFine	0.4833	0.1500	0.4728	0.3208	0.2600	0.2600	0.4623	0.1055	0.1000	0.5890
CFGNExplainer	0.5167	0.1500	0.7199	0.1987	0.5011	0.0000	0.5454	0.3751	0.0000	0.7048
CF ²	0.4667	0.0667	0.6216	0.6189	0.2200	0.0000	0.3706	0.1250	0.0000	0.5991
MixUpExplainer	0.2333	0.1500	0.2064	0.3708	0.1200	0.0800	0.2963	0.0250	0.0750	0.1041
FANS	0.7000	0.0000	0.9311	0.5819	0.7600	0.0000	0.8619	0.4251	0.0000	0.9755

necessity modules ensure that the feature subset contains all features responsible for the prediction and removes those that are not respectively, which result in a more dense or sparse optimal feature subset. Thus, the optimal subset estimated by FANSw/oSF may only contain a subset of features that are responsible for prediction. Removing these features may lead to prediction change (high FID+), while retaining these features may also lead to prediction change (high FID-) since the important features are incomplete. Similarly, the optimal subset estimated by FANSw/oNC may contain redundancy. Retaining these features may keep the prediction unchanged (low FID-) while removing these features the change in prediction is uncertain (low FID+) due to the redundancy.

Next, we compared FANS with FANSw/oSR. As shown in Fig.4(a)(b), the sparsity metric SPA of FANSw/oSR remains stable because of FANS’s necessity module. However, both faithfulness metrics FID+ and FID- decrease. This may be because FANSw/oSR lacks information about predictions from samples similar to the target input when learning the optimal subset of features, which may lead to FANS being affected by unimportant features in the target input. Additional efficiency analyses involving different methods on CIFAR10 are presented in Appendix 7.

7. Efficiency Analysis

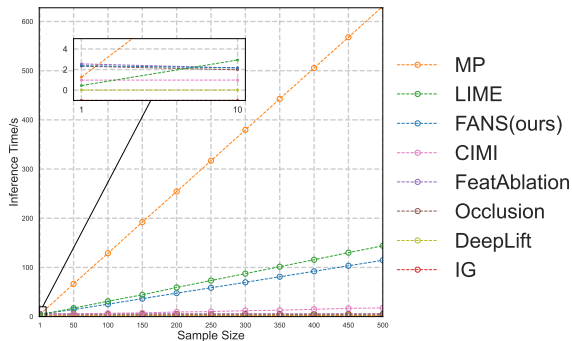


Figure 6. Efficiency analysis on the CIFAR10 dataset.

We evaluate the efficiency of FANS on CIFAR10, in terms of the inference time. We select representative baselines, including optimization-based methods MP, LIME, and CIMI, as well as non-optimization-based methods FeatAblation, Occlusion, DeepLift, and IG.

As shown in Figure 6, the efficiency of FeatAblation, Occlusion, DeepLift, and IG remains stable, as expected since they simply compute gradients or perturbations, enabling parallel computation. However, it is worth noting that when explaining a single sample, FANS is competitive. In contrast, optimization-based methods such as FANS, MP, and LIME tend to have longer inference times, which is expected since they build each optimization instance when explaining each sample. However, FANS is more efficient compared to MP and LIME, probably due to its well-defined objective function without ambiguous trade-off coefficients. Additionally, CIMI adopts mini-batch optimization technology, which further improves its efficiency.

8. Conclusion

This paper presents a Feature Attribution with necessity and sufficiency (FANS) method an explainability method that can better distinguish the contribution of different features to predictions. Compared with the existing methods, this paper first proposes a general perturbative prediction process of ML models. Building upon this process, we incorporate Probability of Necessity and Sufficiency (PNS) into the process of measuring the contribution of features to prediction through perturbations via our proposed dual-stage perturbation test, which follows the Abduction-Action-Prediction counterfactual reasoning paradigm. To generate counterfactual samples, this paper proposes to use a sampling-importance-resampling approach to approximate the required conditional distribution with the observed samples. Experiment results on six mainstream benchmark datasets further evaluate the effectiveness of our proposed FANS. In summary, this paper takes a meaningful step towards machine learning explainability.

9. Impact Statement

This paper proposes a feature attribution method called FANS, which can distinguish the contributions of different features even if the results change the same after perturbation. FANS can be used in medical diagnosis, autonomous driving, and other fields to assist people in understanding the predictions of the model, which have the potential to facilitate the application of existing artificial intelligence technologies in real-world scenarios.

References

- Amara, K., Ying, Z., Zhang, Z., Han, Z., Zhao, Y., Shan, Y., Brandes, U., Schemm, S., and Zhang, C. Graphframex: Towards systematic evaluation of explainability methods for graph neural networks. In Rieck, B. and Pascanu, R. (eds.), *Learning on Graphs Conference, LoG 2022, 9-12 December 2022, Virtual Event*, volume 198 of *Proceedings of Machine Learning Research*, pp. 44. PMLR, 2022. URL <https://proceedings.mlr.press/v198/amara22a.html>.
- Ancona, M., Ceolini, E., Öztireli, C., and Gross, M. Towards better understanding of gradient-based attribution methods for deep neural networks. In *6th International Conference on Learning Representations, ICLR 2018, Vancouver, BC, Canada, April 30 - May 3, 2018, Conference Track Proceedings*. OpenReview.net, 2018. URL <https://openreview.net/forum?id=Sy21R9JAW>.
- Cai, R., Zhu, Y., Chen, X., Fang, Y., Wu, M., Qiao, J., and Hao, Z. On the probability of necessity and sufficiency of explaining graph neural networks: A lower bound optimization approach. *arXiv preprint arXiv:2212.07056*, 2022.
- Chalasanani, P., Chen, J., Chowdhury, A. R., Wu, X., and Jha, S. Concise explanations of neural networks using adversarial training. In *Proceedings of the 37th International Conference on Machine Learning, ICML 2020, 13-18 July 2020, Virtual Event*, volume 119 of *Proceedings of Machine Learning Research*, pp. 1383–1391. PMLR, 2020. URL <http://proceedings.mlr.press/v119/chalasanani20a.html>.
- Dhurandhar, A., Natesan Ramamurthy, K., and Shanmugam, K. Is this the right neighborhood? accurate and query efficient model agnostic explanations. *Advances in Neural Information Processing Systems*, 35:9499–9511, 2022.
- Fong, R. C. and Vedaldi, A. Interpretable explanations of black boxes by meaningful perturbation. In *Proceedings of the IEEE international conference on computer vision*, pp. 3429–3437, 2017.
- Galhotra, S., Pradhan, R., and Salimi, B. Explaining black-box algorithms using probabilistic contrastive counterfactuals. In *Proceedings of the 2021 International Conference on Management of Data*, pp. 577–590, 2021.
- He, K., Zhang, X., Ren, S., and Sun, J. Deep residual learning for image recognition. In *Proceedings of the IEEE conference on computer vision and pattern recognition*, pp. 770–778, 2016.
- Hedström, A., Weber, L., Krakowczyk, D., Bareeva, D., Motzkus, F., Samek, W., Lapuschkin, S., and Höhne, M. M. M. Quantus: An explainable ai toolkit for responsible evaluation of neural network explanations and beyond. *Journal of Machine Learning Research*, 24(34):1–11, 2023. URL <http://jmlr.org/papers/v24/22-0142.html>.
- Kipf, T. N. and Welling, M. Semi-supervised classification with graph convolutional networks. *arXiv preprint arXiv:1609.02907*, 2016.
- Koh, P. W. and Liang, P. Understanding black-box predictions via influence functions. In *International conference on machine learning*, pp. 1885–1894. PMLR, 2017.
- Kokhlikyan, N., Miglani, V., Martin, M., Wang, E., Al-sallakh, B., Reynolds, J., Melnikov, A., Kliushkina, N., Araya, C., Yan, S., et al. Captum: A unified and generic model interpretability library for pytorch. *arXiv preprint arXiv:2009.07896*, 2020.
- Krizhevsky, A., Hinton, G., et al. Learning multiple layers of features from tiny images. 2009.
- LeCun, Y., Bottou, L., Bengio, Y., and Haffner, P. Gradient-based learning applied to document recognition. *Proceedings of the IEEE*, 86(11):2278–2324, 1998.
- Lucic, A., Ter Hoeve, M. A., Tolomei, G., De Rijke, M., and Silvestri, F. Cf-gnnexplainer: Counterfactual explanations for graph neural networks. In *International Conference on Artificial Intelligence and Statistics*, pp. 4499–4511. PMLR, 2022.
- Lundberg, S. M. and Lee, S.-I. A unified approach to interpreting model predictions. *Advances in neural information processing systems*, 30, 2017.
- Luo, D., Cheng, W., Xu, D., Yu, W., Zong, B., Chen, H., and Zhang, X. Parameterized explainer for graph neural network. *Advances in neural information processing systems*, 33:19620–19631, 2020.
- Mueller, S., Li, A., and Pearl, J. Causes of effects: Learning individual responses from population data. *arXiv preprint arXiv:2104.13730*, 2021.

- Pearl, J. Structural counterfactuals: A brief introduction. *Cognitive science*, 37(6):977–985, 2013.
- Pearl, J. Probabilities of causation: three counterfactual interpretations and their identification. In *Probabilistic and Causal Inference: The Works of Judea Pearl*, pp. 317–372. 2022.
- Ribeiro, M. T., Singh, S., and Guestrin, C. ” why should i trust you?” explaining the predictions of any classifier. In *Proceedings of the 22nd ACM SIGKDD international conference on knowledge discovery and data mining*, pp. 1135–1144, 2016.
- Rieger, L. and Hansen, L. K. IROF: a low resource evaluation metric for explanation methods. *CoRR*, abs/2003.08747, 2020. URL <https://arxiv.org/abs/2003.08747>.
- Sen, P., Namata, G., Bilgic, M., Getoor, L., Galligher, B., and Eliassi-Rad, T. Collective classification in network data. *AI magazine*, 29(3):93–93, 2008.
- Shapley, L. S. et al. A value for n-person games. 1953.
- Simonyan, K., Vedaldi, A., and Zisserman, A. Deep inside convolutional networks: Visualising image classification models and saliency maps. *arXiv preprint arXiv:1312.6034*, 2013.
- Simonyan, K., Vedaldi, A., and Zisserman, A. Deep inside convolutional networks: Visualising image classification models and saliency maps. In Bengio, Y. and LeCun, Y. (eds.), *2nd International Conference on Learning Representations, ICLR 2014, Banff, AB, Canada, April 14-16, 2014, Workshop Track Proceedings*, 2014. URL <http://arxiv.org/abs/1312.6034>.
- Springenberg, J. T., Dosovitskiy, A., Brox, T., and Riedmiller, M. A. Striving for simplicity: The all convolutional net. In Bengio, Y. and LeCun, Y. (eds.), *3rd International Conference on Learning Representations, ICLR 2015, San Diego, CA, USA, May 7-9, 2015, Workshop Track Proceedings*, 2015. URL <http://arxiv.org/abs/1412.6806>.
- Sundararajan, M., Taly, A., and Yan, Q. Axiomatic attribution for deep networks. In *International conference on machine learning*, pp. 3319–3328. PMLR, 2017.
- Tan, J., Geng, S., Fu, Z., Ge, Y., Xu, S., Li, Y., and Zhang, Y. Learning and evaluating graph neural network explanations based on counterfactual and factual reasoning. In *Proceedings of the ACM Web Conference 2022*, pp. 1018–1027, 2022.
- Wang, X., Wu, Y., Zhang, A., He, X., and Chua, T.-S. Towards multi-grained explainability for graph neural networks. *Advances in Neural Information Processing Systems*, 34:18446–18458, 2021.
- Watson, D. S., Gultchin, L., Taly, A., and Floridi, L. Local explanations via necessity and sufficiency: Unifying theory and practice. In *Uncertainty in Artificial Intelligence*, pp. 1382–1392. PMLR, 2021.
- Wu, C., Wang, X., Lian, D., Xie, X., and Chen, E. A causality inspired framework for model interpretation. In *Proceedings of the 29th ACM SIGKDD Conference on Knowledge Discovery and Data Mining*, pp. 2731–2741, 2023.
- Xiao, H., Rasul, K., and Vollgraf, R. Fashion-mnist: a novel image dataset for benchmarking machine learning algorithms. *arXiv preprint arXiv:1708.07747*, 2017.
- Yang, M., Zhang, Y., Fang, Z., Du, Y., Liu, F., Ton, J.-F., Wang, J., and Wang, J. Invariant learning via probability of sufficient and necessary causes. In *Thirty-seventh Conference on Neural Information Processing Systems*, 2023a. URL <https://openreview.net/forum?id=K5e5tFZuur>.
- Yang, R., Wang, B., and Bilgic, M. Idgi: A framework to eliminate explanation noise from integrated gradients. In *Proceedings of the IEEE/CVF Conference on Computer Vision and Pattern Recognition*, pp. 23725–23734, 2023b.
- Yeh, C.-K., Hsieh, C.-Y., Suggala, A., Inouye, D. I., and Ravikumar, P. K. On the (in) fidelity and sensitivity of explanations. *Advances in Neural Information Processing Systems*, 32, 2019.
- Ying, Z., Bourgeois, D., You, J., Zitnik, M., and Leskovec, J. Gnnexplainer: Generating explanations for graph neural networks. *Advances in neural information processing systems*, 32, 2019.
- Zeiler, M. D. and Fergus, R. Visualizing and understanding convolutional networks. In *Computer Vision—ECCV 2014: 13th European Conference, Zurich, Switzerland, September 6-12, 2014, Proceedings, Part I 13*, pp. 818–833. Springer, 2014.
- Zhang, J., Luo, D., and Wei, H. Mixupexplainer: Generalizing explanations for graph neural networks with data augmentation. In *Proceedings of the 29th ACM SIGKDD Conference on Knowledge Discovery and Data Mining*, pp. 3286–3296, 2023.

A. Resampling Weight for Approximate Sampling

SIR consists of three steps. 1) Draw samples $\mathbf{v}_1, \dots, \mathbf{v}_k$ from the proposal distribution $Q(\mathbf{X})$. 2) For each \mathbf{v}_i , calculate the weight $w(\mathbf{v}) = \frac{P(\mathbf{v}|\bar{A}_s, \bar{B}_s) \leq c}{Q(\mathbf{v})}$ if $\|\mathbf{v}_s - \mathbf{x}_s\|_p \leq b$ (definition of variable $\tilde{\mathbf{X}}$ in Eq.1) and 0 otherwise. 3) Draw samples from $\mathbf{v}_1, \dots, \mathbf{v}_k$ based on their weights.

Next, we propose a method for estimating $\frac{P(\mathbf{v}|\bar{A}_s, \bar{B}_s)}{Q(\mathbf{v})}$. As the training set of the ML model comes from $P(\mathbf{X})$, we set $Q(\mathbf{X}) := P(\mathbf{X})$, thus $w(\mathbf{v}) = \frac{P(\mathbf{v}|\bar{A}_s, \bar{B}_s) \leq c}{P(\mathbf{v})} = \frac{P(\mathbf{v})P(\bar{A}_s, \bar{B}_s|\mathbf{v})}{P(\mathbf{v})P(\bar{A}_s, \bar{B}_s)} = \frac{P(\bar{A}_s, \bar{B}_s|\mathbf{v})}{P(\bar{A}_s, \bar{B}_s)} = r \cdot P(\bar{A}_s, \bar{B}_s|\mathbf{v})$, where r is a normalization constant.

B. Experimental Setup

B.1. Datasets and Target Models

To evaluate the effectiveness of our proposed FANS, we utilize six datasets with well-trained black box models to be explained on image and graph domains: (1) on three image datasets (MNIST, Fashion-MNIST, CIFAR10), we train three image classification models using LeNet5 architecture (LeCun et al., 1998) for the first two datasets and ResNet18 (He et al., 2016) for the third dataset, and (2) on two citation graphs (Citeseer, Pubmed) and one synthetic graph (BACommunity), we train three node classification models, each consisting of three GCN (Kipf & Welling, 2016) layers, following (Wang et al., 2021). Table 3 summarizes the statistics of six datasets.

- **MNIST** (LeCun et al., 1998) contains grayscale images of the 10 digits.
- **Fashion-MNIST** (Xiao et al., 2017) contains grayscale images of the 10 categories.
- **CIFAR10** (Krizhevsky et al., 2009) contains colour images of the 10 categories.
- **BACommunity** (Ying et al., 2019) consists of two BA-Shapes graphs and includes eight node categories. A BA-Shapes graph contains a Barabási-Albert (BA) graph and “house”-structured network motifs.
- **Citeseer** and **Pubmed** (Sen et al., 2008) contain documents represented by nodes and citation links represented by edges.

B.2. Baselines

We consider two categories of methods, feature-wise attributions and feature subset-wise attributions. Feature-wise attribution methods include:

- **Saliency** (Simonyan et al., 2014) construct contributions using absolute values of partial derivatives.
- **GuidedBP** (Springenberg et al., 2015) sets the gradients and ReLU inputs to zero if they are negative.
- **IntegratGrad** (Sundararajan et al., 2017) average gradients along a linear path between the reference and input.
- **GradShap** (Lundberg & Lee, 2017) approximates SHAP values by stochastic sampling from the reference distribution and computing the expectations of gradients.
- **DeepLift** (Ancona et al., 2018) addresses saturation issues by employing “reference activations” computed during the forward pass with the reference input.
- **IDGI** (Yang et al., 2023b) enhances attribution quality by removing noise in IG-based methods through focused use of gradients along the important direction.

Feature subset-wise attribution methods include:

- **Occlusion** (Zeiler & Fergus, 2014) induces changes in the classifier output through perturbation via sliding a gray square over the input image.
- **LIME** (Ribeiro et al., 2016) quantifies the contributions by using a simplified, interpretable surrogate by fitting the input’s neighborhood.
- **MeaningfulPerturbation(MP)** (Fong & Vedaldi, 2017) optimizes the shape of perturbation masks to minimize input image blurring while maximizing class score decrease.
- **GNNExplainer** (Ying et al., 2019) minimizes the loss by balancing the density penalty and cross-entropy of model prediction on the masked subgraph.
- **PGExplainer** (Luo et al., 2020) extends GNNExplainer by assuming a random Gilbert graph, where edge probabilities are conditionally independent.
- **FeatAblation** (Kokhlikyan et al., 2020) computes attribution by replacing each input feature with a reference and measuring the output difference.
- **ReFine** (Wang et al., 2021) involves edge attribution through pre-training, which optimizes mutual information (MI) and contrastive loss, and edge selection through fine-tuning, which solely maximizes MI.
- **CFGNEExplainer** (Lucic et al., 2022) generates counterfactual explanations by learning a perturbed adjacency matrix that flips the classifier prediction for a node.

Table 3. Statistics of the datasets.

Category	Dataset	# Images	Size	# Classes	
Image	MNIST	70,000	28×28	10	
	Fashion-MNIST	70,000	28×28	10	
	CIFAR10	60,000	32×32	10	
		# Nodes	# Edges	# Features	
Graph	BACommunity	1,400	8,598	10	8
	Citeseer	3,327	4,732	3,703	6
	Pubmed	19,717	44,338	500	3

- **CIMI**(Wu et al., 2023) minimizes the loss by balancing their proposed sufficiency loss, intervention loss, and causal prior loss.
- **MixUpExplainer**(Zhang et al., 2023) mixes explanations with a randomly sampled base structure to address distribution shifting issues.
- **CF²**(Tan et al., 2022) proposes an objective function for optimizing the edge mask, which consists of factual loss, counterfactual loss, and L_1 regularization.

B.3. Evaluation Metrics

It is challenging to evaluate the quality of explanations quantitatively because the ground truth explanations are usually not available. There are six widely used metrics in the literature.

- **Infidelity (INF)**(Yeh et al., 2019) measures the expected mean square error between the dot product of an attribution and input perturbation, and the difference of output after significant perturbation associated with the attribution.
- **IROF (IR)**(Rieger & Hansen, 2020) calculates the area under the curve per class based on the sorted mean importance of iteratively removed feature segments.
- **Fidelity⁺ (FID⁺)** and **Fidelity⁻ (FID⁻)**(Amara et al., 2022) respectively evaluate the proportions of predictions changing and remaining unchanged when features with high attribution scores are removed and retained.
- **Max-Sensitivity (MS)**(Yeh et al., 2019) computes the maximum difference between new and original attributions, where the new attributions correspond to perturbed inputs.
- **Sparseness (SPA)**(Chalasanani et al., 2020) applies the Gini index to the absolute values on the attribution.

- **Recall@N**(Wang et al., 2021) is computed as $\mathbb{E}_{\mathcal{G}} [|\mathcal{G}_s \cap \mathcal{G}_S^*| / |\mathcal{G}_S^*|]$, where \mathcal{G}_s^* is the ground-truth explanatory subgraph. Note that Recall@N in this paper is only suitable for BACommunity since it is a synthetic dataset with known motifs.

B.4. Implementation Details

For the parametric explanation methods (MP, GNNExplainer, PGExplainer, ReFine, CFGNExplainer, CIMI, MixUpExplainer), we conducted a grid search to tune their hyperparameters. For our FANS, we utilized the Adam optimizer and set the learning rate to 0.001 for image datasets and 0.1 for graph datasets. The maximum number of training epochs was set to 50 for image datasets and 30 for graph datasets. The times of perturbation t in Eq. 11 and u in Eq. 13 were both set to 50. while the resampling sizes were set to 1.